ChemPubSoc Europe
DOI: 10.1002/chem.201400373
CHEMISTRY
A European Journal
Full Paper

Green Chemistry

Uncatalyzed Hydroamination of Electrophilic Organometallic Alkynes: Fundamental, Theoretical, and Applied Aspects

Yanlan Wang,[a] Camille Latouche,[b] Amalia Rapakousiou,[a] Colin Lopez,[c] Isabelle Ledoux-Rak,[c] Jaime Ruiz,[a] Jean-Yves Saillard,*[b] and Didier Astruc*[a]

Abstract: Simple reactions of the most used functional groups allowing two molecular fragments to link under mild, sustainable conditions are among the crucial tools of molecular chemistry with multiple applications in materials science, nanomedicine, and organic synthesis as already exemplified by peptide synthesis and "click" chemistry. We are concerned with redox organometallic compounds that can potentially be used as biosensors and redox catalysts and report an uncatalyzed reaction between primary and secondary amines with organometallic electrophilic alkynes that is free of side products and fully "green". A strategy is first proposed to synthesize alkynyl organometallic precursors upon addition of electrophilic aromatic ligands of cationic complexes followed by *endo* hydride abstraction. Electrophilic alkynylated cyclopentadienyl or arene ligands of Fe, Ru, and Co complexes subsequently react with amines to yield *trans*-enamines that are conjugated with the organometallic group. The difference in reactivities of the various complexes is rationalized from the two-step reaction mechanism that was elucidated through DFT calculations. Applications are illustrated by the facile reaction of ethynylcobalticenium hexafluorophosphate with aminated silica nanoparticles. Spectroscopic, nonlinear-optical and electrochemical data, as well as DFT and TDDFT calculations, indicate a strong push–pull conjugation in these cobalticenium– and Fe– and Ru–arene–enamine complexes due to planarity or near-planarity between the organometallic and *trans*-enamine groups involving fulvalene iminium and cyclohexadienylidene iminium mesomeric forms.

Introduction

An important goal in organometallic chemistry and materials science is the incorporation and engineering of organometallic derivatives into nanomaterials towards applications in sensing, electronic polymers, redox catalysts, derivatized electrodes, and nanomedicine.[1] For this purpose, the concept of "click" chemistry involving easy, high-yielding, environmentally benign reactions without side products proposed by Sharpless in 2001[2] has proven to be of considerable utility for the functionalization of compounds towards multiple applications.[3] The most common "click" reactions utilize alkynes and azides that are rather readily introduced into a variety of molecules and a transition-metal catalyst, although the latter is sometimes difficult to completely remove from products.[4]

Here we introduce a new clean, uncatalyzed reaction of cationic cobalt, iron, and ruthenium organometallic alkynes with amines. Amines are among the most important classes of organic molecules,[5] and therefore their use for "click" reactions is desirable. Nucleophilic additions to electron-deficient alkynes[6–10] are mostly catalyzed by transition-metal complexes,[6] but uncatalyzed reactions have also been developed with haloacetylenes[7–9] and other electron-deficient alkynes.[10]

For our purpose, we are using robust cationic 18-electron late transition-metal organometallic compounds in which the alkyne is introduced by *exo*-nucleophilic addition onto a π ligand[11] followed by *endo*-hydride abstraction using commercial trityl hexafluorophosphate [Eq. (1)].[12]

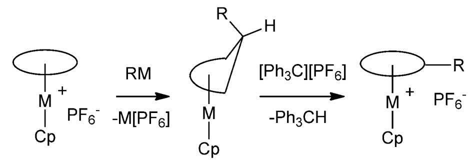

(1)

This sequence of reactions has been conducted with cationic organotransition-metal complexes and functional and nonfunctional carbanions with varied success since the pioneering period of organometallic chemistry and eventually provides substituted organotransition-metal complexes.[11–13] With the

---

[a] Dr. Y. Wang, Dr. A. Rapakousiou, Dr. J. Ruiz, Prof. D. Astruc
ISM, UMR CNRS 5255, Univ. Bordeaux
351 Cours de la Libération, 33405 Talence Cedex (France)
E-mail: didier.astruc@u-bordeaux1.fr

[b] C. Latouche, Prof. J.-Y. Saillard
Institut des Sciences Chimiques de Rennes
UMR CNRS 6226, Université de Rennes 1
35042 Rennes Cedex (France)
E-mail: jean-yves.saillard@univ-rennes1.fr

[c] C. Lopez, Prof I. Ledoux-Rak
LPQM, UMR CNRS 8537, ENS Cachan
61 Avenue du Président Wilson 94230 Cachan (France)

Supporting information for this article is available on the WWW under http://dx.doi.org/10.1002/chem.201400373.

ethynyl group, a single example has been reported with the synthesis of ethynylcobalticenium.[13]

Here we show that this reaction can be made effective and extended inter alia to η^6-arene ligands in 18-electron cationic iron and ruthenium organometallic complexes in which the ethynyl group can be introduced. This strategy makes the ethynyl group sufficiently electrophilic in all cases of coordinated π ligands in cationic complexes to react smoothly with amines, yielding *trans*-enamines without the need of a catalyst and without the formation of any side product [Eq. (2)].

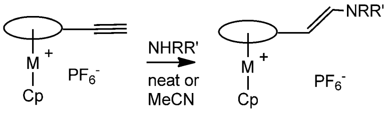

(2)

Fundamental organometallic aspects of this uncatalyzed hydroamination reaction involve on the one hand the intimate mechanism of hydroamination and C–N bond formation for which theoretical studies are most helpful, and on the other hand the physicochemical properties of these new organometallic products that are push–pull *trans*-enamines with specific nonlinear optical properties that are compared among the various iron, ruthenium, and cobalt organometallic complexes and also studied from a theoretical standpoint. The applied aspect that is also developed here and is essential in the overall "click" strategy involves the derivatization of nanomaterials such as nanoparticles by using the facility of the reaction and the ease of access to aminofunctionalized nanomaterials.

Results and Discussion

Synthesis of the ethynyl organometallic complexes

The low-oxidation-state ethynyl organometallic derivatives **4**, **5**, and **6** have been prepared in good yields by adding the ethynyl carbanion in the form of lithium acetylideethylenediamine in THF at 0 °C to the yellow hexafluorophosphate salt of the cationic π-complexes **1**, **2**, and **3**. These *exo*-adducts **4** (red), **5** (orange), and **6** (pink) were obtained as stable solids that were soluble in pentane and characterized by the standard spectroscopic techniques, in particular the strong IR (KBr) absorption around 2090 cm^{-1} for the triple bond, the ethynyl proton in the ^1H NMR spectrum ($CDCl_3$) around $\delta = 3.00$ ppm, the molecular peak in the ESI mass spectra and correct elemental analyses. In the case of **5** and **6**, addition occurs onto the more electrophilic arene ligand. They were submitted to hydride abstraction by using $[Ph_3C][PF_6]$ in CH_2Cl_2 at RT for one hour in order to recover the yellow and orange hexafluorophosphate salts **7**, **8**, and **9** of the functional organometallic cations. These ethynyl derivatives were characterized in the same way including the downfield shift of the ethynyl proton in the ^1H NMR spectrum at around $\delta = 4.44$ ppm and the molecular peaks of the cations of the salts were found in the ESI mass spectra. This sequence of reactions was known with the cobalticenium salt **1**[13] and has been successfully applied for the first time to arene ligands with the ethynyl group to the complexes known $[Fe(Cp)(\eta^6\text{-mesitylene})][PF_6]$, **2**,[14] and $[Ru(\eta^6\text{-benzene})(Cp)][PF_6]$,[15] **3** ($Cp = \eta^5\text{-}C_5H_5$) providing the new complexes **8** and **9** (Scheme 1).

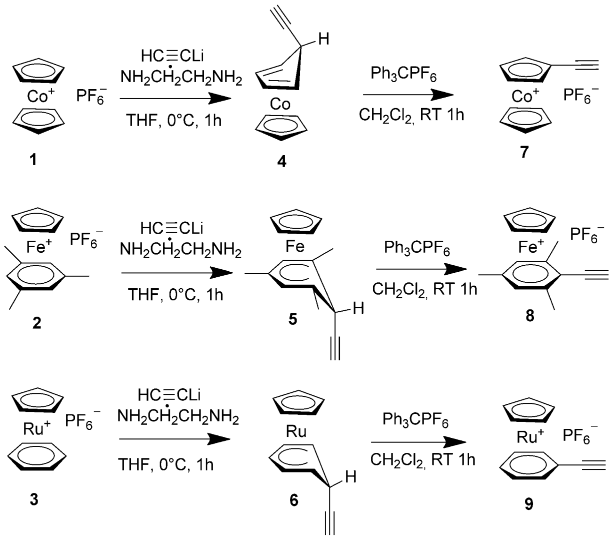

Scheme 1. Synthesis of electrophilic organometallic ethynyl derivatives.

Hydroamination of the ethynyl organometallic derivatives

The ethynyl organometallic derivatives **7**,[13,16] **8**, and **9** react with primary and secondary amines either neat or in acetonitrile solution to give stable *trans*-enamines **10**, **11**, and **12** (Scheme 2). With **7** and **9**, the reaction proceeds more easily than with **8** due to the stereoelectronic effects of the *ortho* methyl groups in the iron complex. For instance, the reaction of **7** and **9** in neat $NH(Et)_2$ proceeds to completion at 35 °C in one hour, but with **8** the reaction needs 24 h to reach quantitative conversion. Comparison of the less bulky amine Et_2NH with iPr_2NH for the same ethynyl organomtallic derivatives shows that the latter reacts much more slowly than the former, which indicates a strong steric effect. Also, the two *ortho* methyl groups in **8** considerably slow down the reaction compared to **7** and **9** vide infra (Table 1). The quantitiative conversion of this reaction was determined by both the NMR spectroscopies and isolated yield.

Figure 1 illustrates the kinetics of the reaction between **7** and excess $NH(nBu)_2$ with an intensity increase of the UV/Vis band at 496 nm and the isosbestic point at 380 nm. This pseudo-first-order reaction proceeds in acetone/$NH(nBu)_2$ (1:1) with a rate constant of $k = 8.45 \times 10^{-3}$ s^{-1}.

Aniline reacts much more slowly than the other amines, as expected due to its lower nucleophilic properties compared to alkyl amines, but a quantitative yield was obtained with **7** when aniline was used as the solvent for two days at 80 °C. A 1:1 mixture of enamine **10 c–a** and its imine tautomer **10 c–b** were obtained.[17] The latter is not favored with alkylamine due to the lack of conjugation with cobalticenium, contrary to the enamines, but with aniline the conjugation of the imine C=N bond with the phenyl ring compensates the lack of conju-

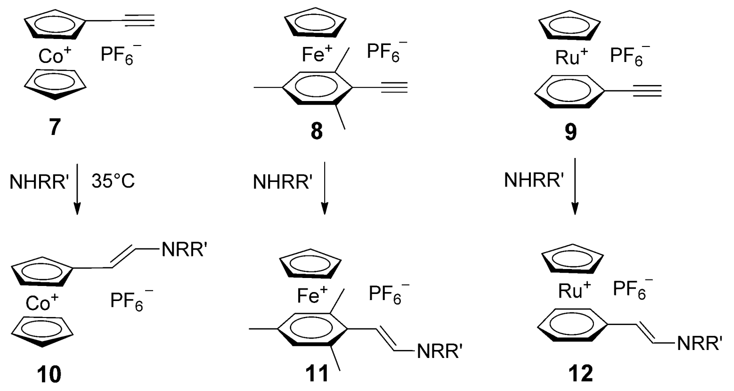

Scheme 2. Reactions of primary and secondary amines with the electrophilic ethynyl organometallic complexes (**10a**: R=R′=*i*Pr; **10b**: R=H, R′=Bu; **10c**: R=H, R′=Ph; **10d**: R=R′=*n*Bu; **10e**: R=R′=Et; **11a**: R=R′=*i*Pr; **11b**: R=R′=Et; **12a**: R=R′=*i*Pr; **12b**: R=R′=Et).

Table 1. Conditions of the hydroamination of the ethynyl organometallic derivatives **7**, **8**, and **9** (neat) to reach quantitative conversions.

Ethynyl derivative	Amine	Product	Reaction *t* [h]	*T* [°C]
7	$i\mathrm{Pr_2NH}$	**10a**	1	35
7	$n\mathrm{BuNH_2}$	**10b**	1	35
7	$\mathrm{PhNH_2}$	**10c**	48	80
7	$n\mathrm{Bu_2NH}$	**10d**	1	35
7	$\mathrm{Et_2NH}$	**10e**	1	35
8	$i\mathrm{Pr_2NH}$	**11a**	24	70
8	$\mathrm{Et_2NH}$	**11b**	24	35
9	$i\mathrm{Pr_2NH}$	**12a**	24	35
9	$\mathrm{Et_2NH}$	**12b**	1	35

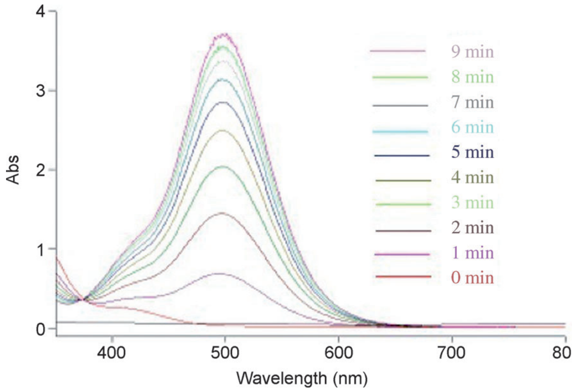

Figure 1. UV/Vis spectra during the reaction of **7** with $\mathrm{NH}(n\mathrm{Bu})_2$ leading to the formation of **10d** in acetone during the first 9 min: $k=8.45\times10^{-3}\ \mathrm{s^{-1}}$, $\lambda_{\mathrm{max}1}=415$, $\lambda_{\mathrm{max}2}=496$ nm; $\varepsilon=1.25\times10^{4}\ \mathrm{L\,mol^{-1}\,cm^{-1}}$.

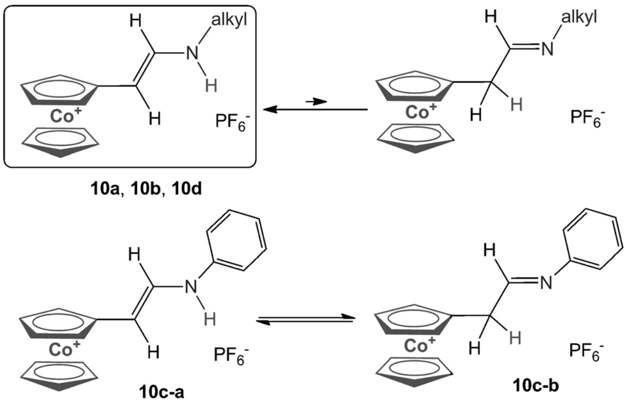

Figure 2. Cobalticenium–enamine–imine tautomerism favored only with aryl amines.

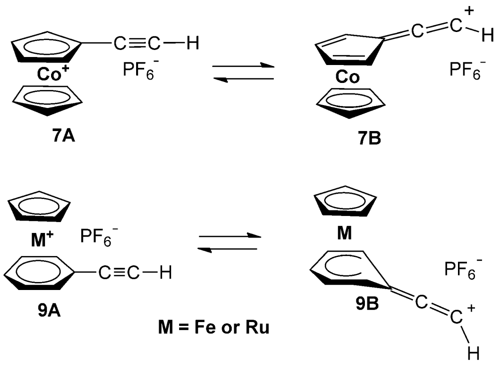

Figure 3. Structures of the electrophilic organometallic alkynes.

gation with cobalticenium (Figure 2). These assignments were made using ^{1}H and ^{13}C NMR spectroscopy of these enamine complexes.

We know that the deprotonation of $[\mathrm{FeCp(C_6Me_6)}][\mathrm{PF_6}]$[18a,b] is much easier than that of $[\mathrm{CoCp(C_5Me_5)}][\mathrm{PF_6}]$,[18c] which is due to the greater positive charge on the benzenic ligand of the iron complex than on the formally anionic permethylated cyclopentadienyl ligand of the cobalt complex. Along this line, one might have expected a faster nucleophilic attack onto the ethynylarene ligand than onto the ethynylcyclopentadienyl ligand, but the opposite is observed. If the reaction of the amines on the ethynyl derivatives would be under charge control, the mesomeric forms in which the positive charge is localized on the second alkyne carbon should be considered (Figure 3), but the calculation will show that the amine attack is not the rate-limiting step. The slightly more stabilizing charge-delocalized structure in the fulvalene ligand, hence with a higher weight of this structure, than in the cyclohexadienylidene ligand is due to a larger ligand folding angle in the latter (Figure 3).[19] The calculation will show, however, that this influence on the conjugation is in fact minimal. The much more serious inhibiting factor is the stereoelectronic steric effect of the two *ortho* methyl groups, especially the steric effect because the calculations will show that the rate-limiting step involves proton transfer onto the sterically protected *exo*-cyclic carbon (vide infra). The electron-donating methyl substituents also decrease the positive charge on the alkyne ligand, which disfavors the reactivity of **8** relative to that of **9**. In summary the stereoelectronic effect of the two *ortho* methyl groups in **8** strongly slows down the reaction with the amines, whereas the opposite effect involving the difference of stabilization of the product between the fulvalene–iminium in **7** and cyclohexadienylidene–iminium in **8** and **9** is much less significant.

Theoretical calculations on the reactions of amines on the electrophilic alkynyl complexes

To shed light on the mechanism of the reaction of amines with the ethynyl derivatives of Scheme 1, we have carried out DFT calculations at the B3PW91/LANL2DZ (see Computational details in the Experimental Section) on the attack of ammonia to $[Co(\eta^5\text{-}C_5H_4CCH)(Cp)]^+$ and $[M(\eta^6\text{-}C_6H_5CCH)(Cp)]^+$ (M = Fe, Ru). We first describe the $NH_3+[Co(\eta^5\text{-}C_5H_4CCH)(Cp)]^+$ (i.e. the cation of **7**) system, the two-step energy profile of which is shown in Figure 4 and relevant structural data of the corresponding extrema are provided in Table 2. The structure of the starting cation of **7**, $[Co(\eta^5\text{-}C_5H_4CCH)(Cp)]^+$ exhibits a pentahapto coordination mode of the substituted ring with a Co–C_{ipso} bond of 2.08 Å that is only slightly longer than the average of the four other Co–C bonds (2.05 Å). Whereas the C_{ipso}–C_α distance (1.42 Å) is consistent with the existence of some conjugation, the C_α–C_β (1.22 Å) is indicative of a regular triple bond and the $C_\alpha C_\beta H$ unit is linear. Thus, the weight of the **7B** Lewis structure in Figure 3 is very small with respect to that of **7A**. Consistently, the C_β natural atomic charge (−0.09) does not show any particular electrophilic character of this atom (it is in fact equal to the C_α charge) and the MO diagram of $[Co(\eta^5\text{-}C_5H_4CCH)(Cp)]^+$ resembles that of cobalticenium with in addition the orbitals associated with the C≡C bond. The two highest occupied MOs can be identified as being the two π_{CC} orbitals, whereas the lowest vacant MO with a significant π^*_{CC} contribution is the LUMO+2 that lies 2.16 eV above the LUMO and 6.53 eV above the HOMO, and is localized 9 and 22% on C_α and C_β, respectively (see the Supporting Information).

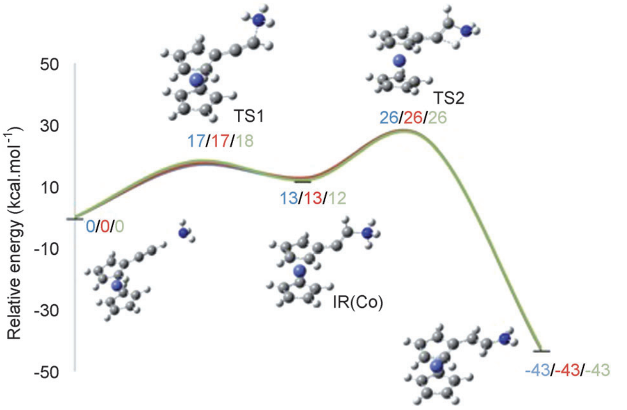

Figure 4. Computed free-energy profiles (at 298 K) for the addition reaction of NH_3 to $[Co(\eta^5\text{-}C_5H_4CCH)(Cp)]^+$ and $[M(\eta^6\text{-}C_6H_5CCH)(Cp)]^+$ (M = Fe, Ru). The blue, red, and green colors correspond to the cobalt, iron, and ruthenium systems, respectively. The molecular structures that are shown correspond to the energy extrema of the cobalt system.

Table 2. Selected metrical data computed for the extrema of the three energy curves shown in Figure 4.[a]

	Co R	TS$_1$	IR	TS$_2$	P	**10** from X-ray[b]
M–C_{ipso}	2.080	2.224	2.218	2.132	2.165	2.130
other M–C[c] (range)	2.049–2.053	2.014–2.058	2.013–2.054	2.032–2.053	2.027–2.055	2.005–2.035
M–C(Cp) (av.)	2.056	2.065	2.063	2.057	2.064	2.028
C_{ipso}–C_α	1.417	1.377	1.406	1.443	1.433	1.432
C_α–C_β	1.219	1.263	1.317	1.337	1.369	1.364
C_β–N	–	1.831	1.520	1.479	1.349	1.336
C_{ipso}–C_α–C_β	177	169	128	127	123	123
$\Sigma\alpha_N$	–	–	–	–	359	360
	Fe R	TS$_1$	IR	TS$_2$	P	
M–C_{ipso}	2.139	2.305	2.344	2.222	2.242	
other M–C[c] (range)	2.104–2.112	2.079–2.121	2.086–2.128	2.089–2.121	2.087–2.117	
M–C(Cp) (av.)	2.063	2.061	2.056	2.063	2.062	
C_{ipso}–C_α	1.423	1.381	1.398	1.436	1.439	
C_α–C_β	1.218	1.263	1.313	1.334	1.369	
C_β–N	–	1.833	1.519	1.480	1.349	
C_{ipso}–C_α–C_β	178	168	135	134	124	
$\Sigma\alpha_N$	–	–	–	–	359	
	Ru R	TS$_1$	IR	TS$_2$	P	
M–C_{ipso}	2.275	2.447	2.453	2.352	2.373	
other M–C[c] (range)	2.239–2.243	2.214–2.251	2.211–2.254	2.225–2.252	2.223–2.242	
M–C(Cp) (av.)	2.199	2.200	2.202	2.200	2.200	
C_{ipso}–C_α	1.424	1.379	1.399	1.438	1.440	
C_α–C_β	1.218	1.262	1.314	1.334	1.367	
C_β–N	–	1.825	1.518	1.480	1.350	
C_{ipso}–C_α–C_β	178	173	134	134	124	
$\Sigma\alpha_N$	–	–	–	–	359	

[a] Distances in Å and angles in °. **R** and **P** are the organometallic ethynyl reactant and enamine product, respectively. X-ray data of the enamine complex **10a** are reported for direct comparison with the computed **P(Co)** values. [b] Values averaged on the two (slightly different) independent molecules existing in the crystal unit cell.[16d] [b] Distances corresponding to the substituted ring.

The ammonia molecule adds to C_β from a "top" side approach (Figure 4). Despite the apparent weak electrophilicity of this atom, the NH_3 addition does not require a very large activation energy (17 kcal mol^{-1}), thanks to the significant polarizability of **7**, which allows it to evolve, during the first stage of the addition reaction, towards an activated structure in which the **7B** Lewis formula of Figure 3 has a nonnegligible weight. This is clearly evidenced by the geometry of the first transition state **TS_1(Co)**, which exhibits a Co–C_{ipso} bond significantly larger than the average of the other four Co–C bonds (2.22 vs. 2.04 Å). Consistently, the C_{ipso}–C_α distance (1.38 Å) in **TS_1(Co)** approaches that of a double bond. The $[Co\{\eta^5\text{-}C_5H_4CC(H)NH_3\}(Cp)]^+$ adduct **IR(Co)** is formed as a high-energy intermediate (Figure 4 and Table 2). The metrical data of Table 2 suggest **TS_1(Co)** is best described with by Lewis formula **A** of Figure 5 (note in particular the bond angle of 128° at C_α, consistent with sp^2 hybridization), with some minor participation of the **B** formula. The MO diagram of **IR(Co)** (see the Supporting Information) supports this view, with the HOMO and HOMO-1 that can be described as the C_α lone pair and the π_{CC} orbital mixed with a 3d(Co) AO, respectively.

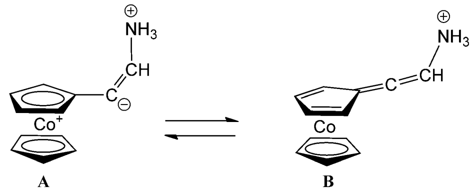

Figure 5. Lewis structures of the reaction intermediate $[Co\{\eta^5\text{-}C_5H_4CC(H)NH_3\}(Cp)]^+$ **IR(Co)**.

The second step of the reaction consists of a proton transfer between N and C_α. With a computed activation barrier of 26 kcal mol^{-1}, this is the rate-determining step of the reaction that is markedly exothermic, the final product being more stable than the reactants by 43 kcal mol^{-1}. The metrical data of the enamine cobalticenium complex are in a very good agreement with the corresponding X-ray values of **10 a**,[16d] which are also reported in Table 2 for comparison. In particular, both structures exhibit a rather long Co–C_{ipso} bond, a rather short C_β–N distance and a near planar nitrogen bond system. These features are consistent with significant participation of **10 B** Lewis structure (vide infra).

The reaction of NH_3 with the group-8 ethynyl derivatives $[M(\eta^6\text{-}C_6H_5CCH)(Cp)]^+$ (M = Fe, Ru) leads to results that are quite similar to those obtained for the cobalt species (see Figure 4 and Table 2) and therefore will not be detailed here. The energetic data computed for the three reactions are surprisingly almost identical, the activation and reaction free energies differing by less than 2 kcal mol^{-1}, a value hardly significant at our level of modelization. Inclusion of solvent effects through the PCM model has almost no effect on these values, neither has the basis set quality or the inclusion of dispersion corrections (see Computational details in the Experimental Section).

Organometallic *trans*-enamine structures

The enamine **10 a** (Figure 6) is a deep-red complex, which indicates a strong conjugation between the organocobalt moiety and the enamine function involving a push–pull electronic structure between the nitrogen donor and the cationic cobalt acceptor. This push–pull structure is confirmed by the UV/Vis spectra, the nonlinear optical properties and the cyclic voltammetry. Likewise, the orange enamines **11** and **12** are more colored than their light yellow (Fe) and white (Ru) precursors.

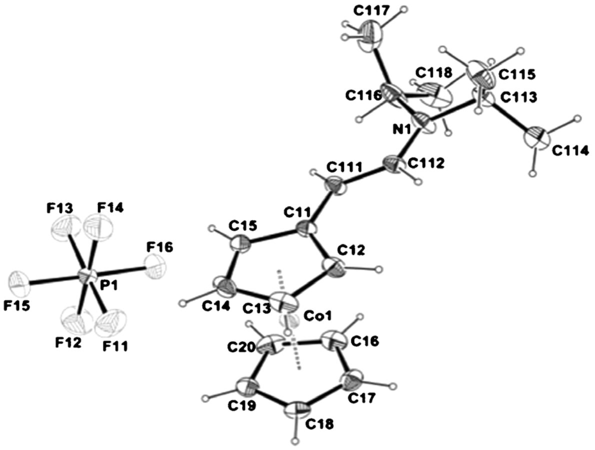

Figure 6. X-ray diffraction structure of the enamine **10 a** with 50 % probability ellipsoids.[16d]

Cyclic voltammetry

The cyclic voltammetry (CV) of the ethynyl and enamine compounds derived from **1** and **2** show, as for the parent complexes **1** and **2**, a chemically and electrochemically reversible reduction wave corresponding to the reduction from 18- to 19-electron complexes. The potential of this wave reflects the electronic influence of the alkynyl and enamine substituent on the redox orbital of the parent complex. The CVs have been recorded under identical conditions to evaluate the comparison of the substituent influence (Table 3 and Figure 7). For both the Co and Fe sandwiches, the introduction of the ethynyl group decreases the redox potential by 170 mV, reflecting a strong electron-withdrawing character of the ethynyl group in **7** and **8**. The introduction of the *trans*-enamine substituent undergoes a slightly different result for the Co and Fe complexes **10 a** and **11 a**, respectively. Whereas the *trans*-enamine shifts the redox potential of the Co complex cathodically by 170 mV with respect to cobalticenium, and 340 mV with respect to ethynylcobalticenium, **7**, this cathodic shift is only 80 mV for the Fe complex **11 a** and 250 mV compared to the ethynyl derivative **8**. This difference of behavior may illustrate the slightly stronger conjugation of the enamine with cobalticenium in **10 a** than with the Fe complex **11 a**. Comparison of the computed electron affinities (EA in Table 3) follows the same trend (decrease of EA of 0.91 eV from **7** to **10 a** and only 0.79 eV from $[Fe(\eta^6\text{-}C_6H_5CCH)(Cp)]^+$, the cation of **8**, to $[Fe(\eta^6\text{-}C_6H_5CH{=}CH\text{-}NH_2)(Cp)]^+$, the demethylated cation of **11 a**, although to a weaker extent than for the CV data, probably again because of the presence of the *ortho* methyl groups in **11 a**.

Table 3. Compared cyclic voltammograms of **1**, **7**, and **10a** and **2**, **8**, and **11a**.[a]

Compound	$E_{1/2}$ [V]	ΔE [mV]	E_A [eV]
1	−0.87	60	−5.47
7	−0.70	75	−5.62
10a	−1.04	60	−4.71
2	−1.43	60	−4.94
8	−1.26	30	−5.05
11a	−1.51	70	−4.26

[a] Under identical conditions (2 mm) with decamethylferrocene, $[Fe(Cp^*)_2]$ ($Cp^* = \eta^5\text{-}C_5Me_5$) as the internal reference. Solvent: DMF; temperature: 293 K; supporting electrolyte: $[nBu_4N][PF_6]$ 0.1 m; working and counter electrodes: Pt; reference electrode: Ag; scan rate: 0.200 $V\,s^{-1}$. The corresponding computed electron affinities (EA) of the free cations are also provided for comparison.

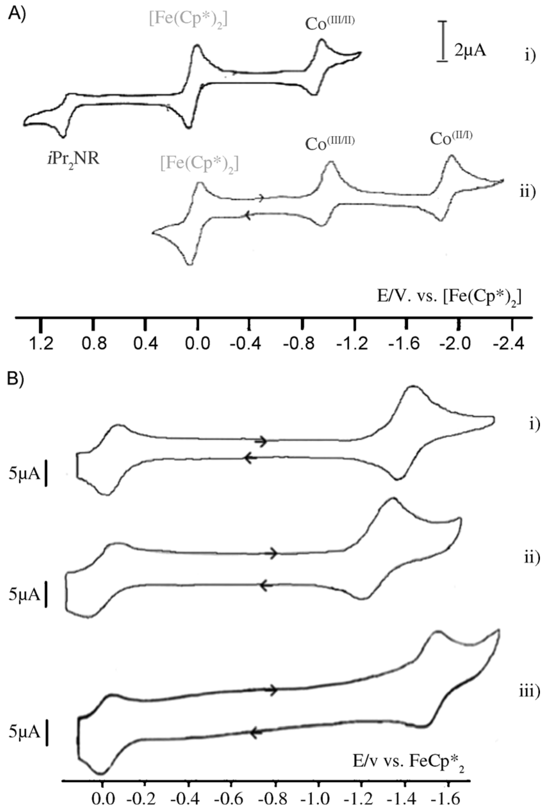

Figure 7. A) i) CV of **10a** (2 mm) obtained at a Pt electrode at 20 °C in CH_2Cl_2; supporting electrolyte: $[nBu_4N][PF_6]$. Anodic wave: $iPr_2N^{0/+}$: $E_{1/2(irrev)} = 1.04$ V ($\Delta E_p = 65$ mV), $Co^{III/II}$ wave: $E_{1/2(rev)} = -1.04$ V ($\Delta E_p = 65$ mV) vs. $[Fe(Cp^*)_2]^{0/+}$ ($Cp^* = \eta^5\text{-}C_5Me_5$). ii) CV of **10a** (2 mm) obtained at a Pt electrode at 20 °C in THF; supporting electrolyte $[nBu_4N][PF_6]$. $Co^{III/II}$ wave: $E_{1/2(rev)} = -1.10$ V ($\Delta E_p = 65$ mV); $Co^{II/I}$ wave: $E_{1/2(rev)} = -2.13$ V ($\Delta E_p = 70$ mV) vs. $[Fe(Cp^*)_2]^{0/+}$. Under the same conditions, the $Co^{III/II}$ wave for the compound **10a** in DMF was obtained: $E_{1/2(rev)} = -1.04$ V ($\Delta E_p = 60$ mV) as in Table 3. B) i) CVof **2**, $Fe^{II/I}$ wave: $E_{1/2(rev)} = -1.43$ V ($\Delta E_p = 60$ mV); ii)- CV of **8**, $Fe^{II/I}$ wave: $E_{1/2(rev)} = -1.26$ V ($\Delta E_p = 30$ mV); iii) CV of **11a**, $Fe^{II/I}$ wave: $E_{1/2(rev)} = -1.51$ V ($\Delta E_p = 70$ mV) under identical conditions (2 mm) with decamethylferrocene $(Fe(Cp^*)_2)$ as the internal reference. Solvent: DMF; temperature: 293 K; supporting electrolyte: $[nBu_4N][PF_6]$ 0.1 m; working and counter electrodes: Pt; reference electrode: Ag; scan rate: 0.200 $V\,s^{-1}$. The values are gathered in Table 3.

UV/Vis spectroscopies

The cobalticenium enamine complexes **10** are deep-red colored, and the iron and ruthenium enamines **11** and **12** are orange complexes, which indicates strong conjugation and participation of the fulvalene–iminium mesomeric form in **10** and cyclohexadienylidene–iminium form **11**–**12B**.

As shown in Figure 8A and Table 4, compound **1** shows peaks at 325 and 405 nm under UV/Vis and ethynylcobalticenium, **7**, similarly shows two absorptions at 335 and 413 nm. Compound **10a** shows another absorption at 499 nm besides the two original small peaks at 324 and 422 nm compared with the two starting materials. The weak absorption around 420 nm is assigned to a d–d* transition of cobalticenium for the three complexes.[20] The new peaks at 499 nm for cobalticenium–enamine, **10a**, is partly related to the conjugation between cobalticenium and the amine group through the C=C bond (see the TDDFT results in the section entitled 'Comparison of the electronic structures of the organometallic enamine complexes and of their physicochemical properties'). The weak peak around 420 nm, related to the d–d* transition of cobalticenium is on the shoulder of the main absorptions at 499 nm for all the cobalticenium–enamine complexes.

Figure 8B and Table 4 show the compared UV/Vis spectra of **2**, **8**, and **11a**, in acetone. There are two typical absorptions in the area of 382–394 and 435–467 nm for the three complexes. There is no new absorption observed for the complex **11a**

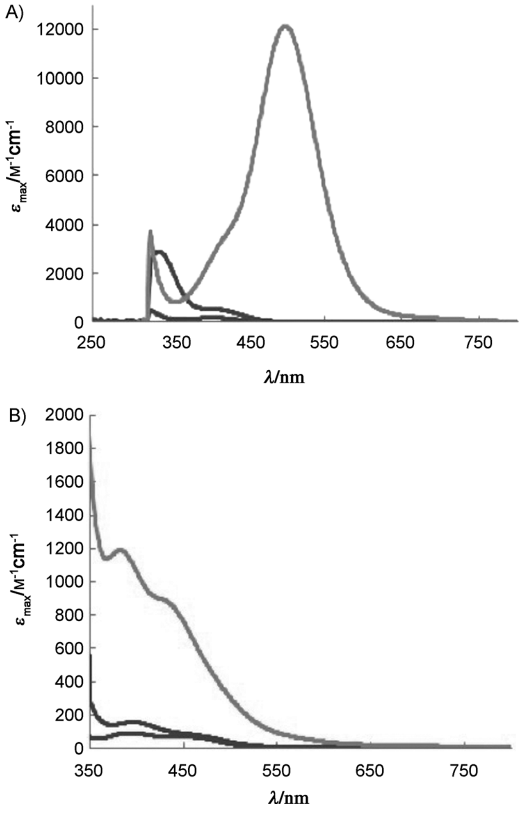

Figure 8. A) Compared UV/Vis spectra for **1** (bottom), **7** (middle), and **10a** (top) in acetone. B) Compared UV/Vis spectra of **2** (bottom), **8** (middle), and **11a** (top) in acetone.

Table 4. UV/Vis absorptions of complexes **7**–**11**, λ = wavelength in nm (molar extinction coefficient, $mol^{-1}\,cm^{-1}$) in acetone.

Compound	$\lambda_{max\,1}$	$\lambda_{max\,2}$	$\lambda_{max\,3}$	Compound	$\lambda_{max\,1}$	$\lambda_{max\,2}$
cobalticenium PF_6(**1**)	325 (501)	405 (195)	–	[Fe(Cp)(η^6-mesitylene)]PF_6(**2**)	392 (97)	457 (77)
ethynylcobalticenium PF_6(**7**)	335 (2913)	413 (460)	–	[Fe(η^6-ethynylmesitylene)(Cp)] PF_6(**8**)	394 (156)	469 (78)
cobalticenium–enamine PF_6 (**10 a**)	324 (3521)	422 (780)	499 (12 500)	[Fe(Cp)(η^6-mesitylene)] enamine PF_6 (**11 a**)	382 (817)	435 (613)

after hydroamination with respect to the cobalticenium analogues. However, the intensities of the two absorptions are increased, and λ_{max} is shifted to lower wavelength than for the two starting materials.

Nonlinear optics

The quadratic nonlinear optical (NLO) properties of compounds **10 a**, **11 a**, and **12 a** have been investigated at ENS Cachan by using two techniques, Electric-Field Induced Second Harmonic Generation[21] (EFISH) that provides information on the scalar product $\mu\beta_{EFISH}$ of the permanent dipole moment μ and of the dipolar component β_{EFISH} of the molecular hyperpolarizability tensor β, and Harmonic Light Scattering (HLS)[22] that measures the value of the whole β tensor (including not only its dipolar part, but also an octupolar contribution) (Table 5).

The HLS technique[22] involves the detection of the incoherently scattered second harmonic light generated by a solution of the molecule under laser irradiation, leading to the measurement of the spatial average mean value of the $\beta\times\beta$ tensor product, $<\beta_{HLS}>$. Using the low-energy, nonresonant incident wavelength of 1.907 μm, prevents any parasitic contribution, such as 2-photon induced fluorescence, to the second harmonic signal.

The negative $\mu\beta_{EFISH}$ values indicate that the dipole moment of the first excited state is weaker than that of the ground state. This can be possibly explained by the inversion of the sign between the dipole of the ground state, dominated by the **10 a**, **11 a**, and **12 a** forms on the left side of Figure 9 and that of the intramolecular charge transfer, excited state dominated by the iminium forms (**10 B**, **11 B**, and **12 B** in Figure 9). The higher absolute value of $\mu\beta_{EFISH}$ for **10 a** is related to the slightly better conjugation between the amino NRR′ donor group and the cobalt moiety than in their Fe and Ru counterparts. These "dipolar" NLO data confirm the conclusions drawn from spectrometric data. This trend is not observed for β_{HLS}, but it must be pointed out that in these hyperpolarizibility values measured by HLS, the octupolar contribution is dominant in most cases. The higher number of π electrons for compounds **11 a** and **12 a** as compared to **10 a** may significantly increase this octupolar contribution, resulting in higher β_{HLS} values for these Fe and Ru complexes (Table 5).

Table 5. Quadratic hyperpolarizabilities β_{HLS} (resp. $\mu\beta_{EFISH}$) measured at 1.9 μm inferred from harmonic light scattering (resp. EFISH technique), for compounds **10 a**, **11 a**, and **12 a**.

Sample	β_{HLS}[a] (10^{-30} esu)	$\mu\beta_{EFISH}$ (10^{-48} esu)
10 a	88	−105[b]
11 a	166	−94[c]
12 a	135	−71[c]

[a] For HLS, 10^{-2} M $CHCl_3$ were used and their NLO response was compared to that of with ethyl violet at the same concentration as the reference. [b] These data were obtained by means of EFISH measurements at 1.91 mm incident wavelength and 10^{-2} M $CHCl_3$ solutions. [c] These data were obtained by means of EFISH measurements at 1.91 mm incident wavelength and 0.7×10^{-2} M $CHCl_3$ solutions.

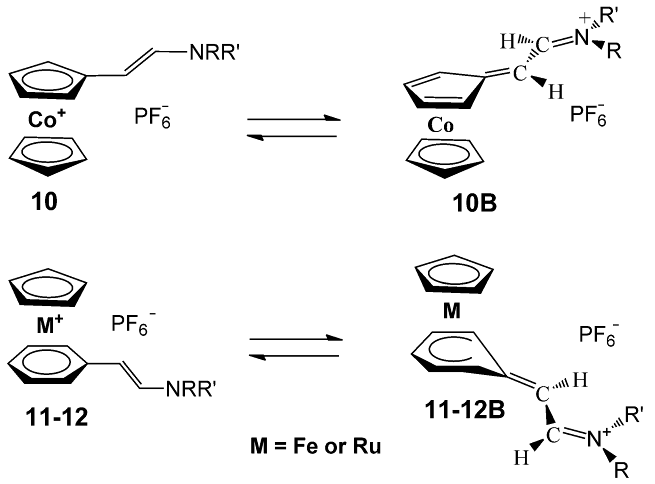

Figure 9. Structures of the *trans*-enamines involving the iminium mesomeric forms in **10** and **11**–**12**.

Comparison of the electronic structures of the organometallic enamine complexes and of their physicochemical properties

Since the computed Fe and Ru systems provide very similar results, only the Fe enamine is compared below to its Co relative. Relevant structural data of the computed models [Co(η^5-$C_5H_4CHCHNH_2$)(Cp)]$^+$ and [Fe(η^6-$C_6H_5CHCHNH_2$)(Cp)]$^+$ are provided in Table 2 and their optimized geometries are shown in Figure 10, together with some computed Wiberg indices. They indicate that both Lewis structures of Figure 9 have to be considered, the iminium form having the lowest, but still substantial, statistical weight. Unsurprisingly, the partial C_{ipso} decoordination does not alter the planarity of the C_5 ring in the cobalt enamine, whereas it is associated with a 16° folding of the C_6 ring in the iron relative. Nevertheless, the amount of conjugation along the enamine chain is found to be quite similar in both compounds, the cobalt derivative being only slightly more conjugated.

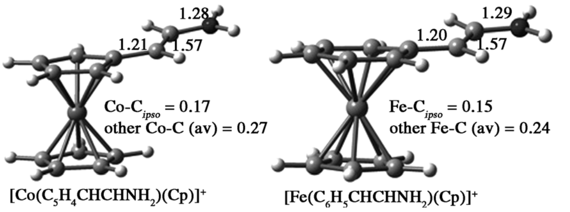

Figure 10. Optimized geometries and relevant computed Wiberg indices of [Co(η^5-$C_5H_4CHCHNH_2$)(Cp)]$^+$ and [Fe(η^6-$C_6H_5CHCHNH_2$)(Cp)]$^+$. All the M–C Wiberg indices correspond to the substituted rings.

Consistently, the MO diagrams of both organometallic enamines (Figure 11) are related with, however, some differences. Their HOMO can be described as the antibonding combination of the π_{CC} orbital with the 2p$_z$(N) orbital that contains the nitrogen lone pair. This HOMO lies far above the two highest members of the "t_{2g}" set associated with the three 3d lone pairs. The two lowest vacant orbitals are the two antibonding 3d(metal)–ligand combinations (the "e_g*"-type orbitals). Whereas the compositions of the orbitals described above are comparable in the Co and Fe derivatives (see the Supporting Information), their energies are somewhat different. This is due mainly to the energy difference between the 3d AOs of Co and Fe that tend to stabilize the "t_{2g}" and "e_g*" sets in the cobalt derivative with respect to those in the iron one. On the other hand, the HOMO energy is hardly changed when going from the Co to the Fe enamine since in both complexes this orbital is mainly localized on the $C_\alpha C_\beta N$ chain. The result is that the HOMO–LUMO gap of the Co derivative is lower than that of its Fe relative.

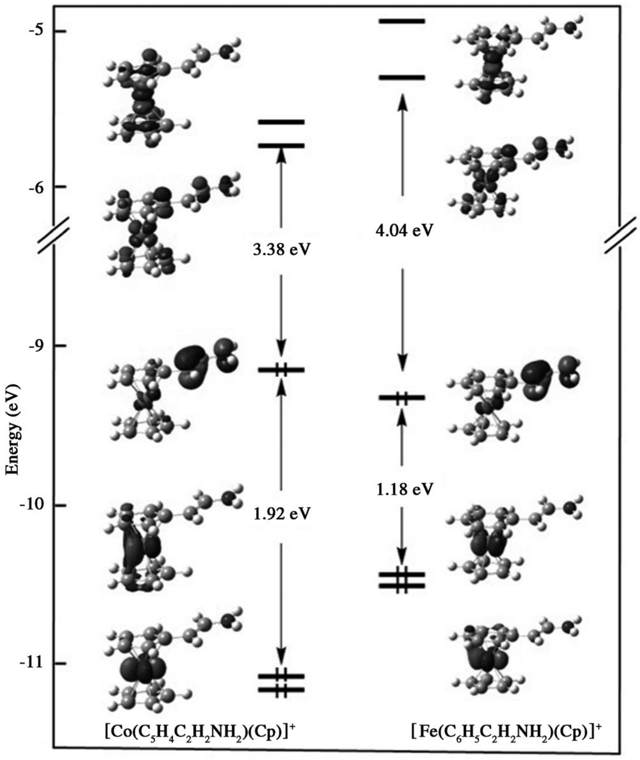

Figure 11. The frontier MO diagrams of [Co(η^5-$C_5H_4CHCHNH_2$)(Cp)]$^+$ and [Fe(η^6-$C_6H_5CHCHNH_2$)(Cp)]$^+$.

The lowest HOMO–LUMO gap found for the Co derivative correlates with the calculated electron affinities of [Co(η^5-$C_5H_4CHCHNH_2$)(Cp)]$^+$ and [Fe(η^6-$C_6H_5CHCHNH_2$)(Cp)]$^+$ (−4.96 and −4.48 eV, respectively. Similar values were computed for the cations of **10a** and **11a** (Table 3). These values are in full consistency with the corresponding $E_{1/2}$ values, as well as those computed for all the cations of the compounds listed in Table 3.

TDDFT calculations on the models [Co(η^5-$C_5H_4CHCHNH_2$)(Cp)]$^+$ and [Fe(η^6-$C_6H_5CHCHNH_2$)(Cp)]$^+$ found that both complexes have related optical transitions in the visible region, but those of the iron complex are blueshifted, because these transitions have non-negligible "t_{2g}" to "e_g*" character. Moreover the computed oscillator strengths of the Fe complex in this absorption region are much less important than those of the Co relative. This is exemplified by the simulated visible absorption spectra of these two models that are shown in Figure 12. In the case of the Co derivative, the major transition of lowest energy is computed at 498 nm. It is mainly of "t_{2g}"→"e_g*" character (66 %) with non-negligible HOMO→LUMO admixture (29 %). This latter contribution tends to reduce the nitrogen lone pair and the π(CC) characters (HOMO) to the profit of the complexed ring (LUMO) in the excited state. This is consistent with the suggestion taken out from the NLO results (see above) of a larger weight of the iminium form **10B** in the excited state.

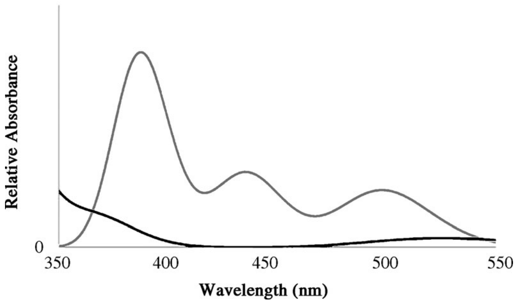

Figure 12. Simulated absorption spectra of [Co(η^5-$C_5H_4CHCHNH_2$)(Cp)]$^+$ (top) and [Fe(η^6-$C_6H_5CHCHNH_2$)(Cp)]$^+$ (bottom) from TDDFT calculations.

The same transition is found at 526 nm for the Fe derivative, but with much lower oscillator strength. The DIPA cation of compound **10a** exhibits a simulated spectrum similar to its unsubstituted [Co(η^5-$C_5H_4CHCHNH_2$)(Cp)]$^+$ relative. Its two major transitions of lowest energy are computed at 498 and 435 nm. These values fit quite well with the corresponding experimental λ_{max} values recorded for **10a** (Figure 8, Table 4).

Derivatization of aminated silica with cobalticenium enamine termini

Given the ease and mild conditions of the uncatalyzed reaction between **7** and primary and secondary amines, the functionali-

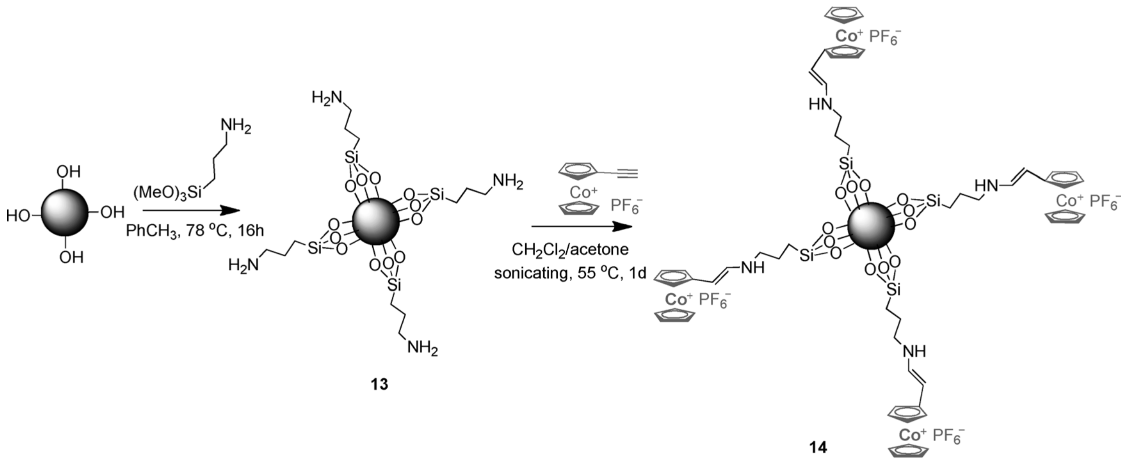

Scheme 3. Derivatization of aminated silica nanoparticles with cobalticenium.

zation of nanomaterials to which the amino groups were attached was investigated. First the reaction between aminated silica was examined, because silica nanoparticles (SiO_2NPs) are easily accessible commercial nanomaterials. MT-ST SiO_2NPs (12 nm diameter) were modified upon reaction with 3-(trimethoxysilyl)propylamine, then after appropriate treatment the known[24] primary amine-terminated SiO_2NPs **13** in CH_2Cl_2/acetone (1:1) was reacted with excess **7** under sonication at 55 °C giving an air-stable, thermally robust nanomaterial **14** (Scheme 3). The SiO_2NPs **13** was reported to contain around 250 amino groups, thus since the IR spectrum of **14** no longer contains the $-NH_2$ bands at 3305 and 3368 cm^{-1} but only the secondary amine band at 3275 cm^{-1} indicating completion of the reaction, we believe that **14** also contains around 250 enamine–cobalticenium groups. Derivatization of other aminated nanomaterials, such as polymers and dendrimers, by hydroamination of electrophilic organometallic alkynes have also been conducted and will be reported in due course.

During this reaction color change from yellow to deep violet was the indication of cobalticenium–enamine formation as with simple molecular amines. After centrifugation and decantation, this deep-violet precipitate was characterized by IR (1621 cm^{-1}, $\nu_{CH=CH}$ and 832 cm^{-1}, ν_{PF6}) and UV/Vis spectroscopy with the appearance of the strong absorption at 502 nm and by cyclic voltammetry at a Pt electrode as a suspension in DMF showing a single reversible wave (with adsorption) at $E_{1/2}$(rev) = −0.94 V (ΔE_p = 65 mV) vs. $[Fe(Cp^*)_2]^{+/0}$ that is characteristic for the $Co^{III/II}$ redox interchange of cobalticenium derivatives (Figure 13).

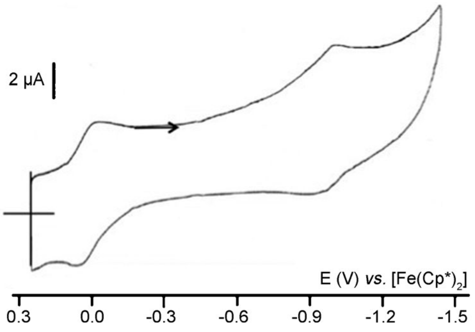

Figure 13. Cyclic voltammetry of cobalticenium–enamine-terminated SiO_2NPs (10 mg mL^{-1}) recorded as a suspension in DMF at a Pt electrode (25 °C); supporting electrolyte: $[nBu_4N][PF_6]$. $Co^{III/II}$ wave: $E_{1/2}$(rev) = −0.94 V (ΔE_p = 65 mV) vs. $[Fe(Cp^*)_2]^{0/+}$.

Conclusion

Access to ethynyl derivatives in which the ethynyl group is attached to and conjugated with a hydrocarbon ligand of various cationic organometallic complexes has been extended to arene organometallic complexes. It allows letting these complexes react with amines resulting in clean, mild, and uncatalyzed hydroamination quantitatively yielding *trans*-enamine products. Although the reactions of nucleophiles with haloalkynes have long been examined in organic chemistry, the organometallic "Umpolung" of the alkyne reactivity allowing the formation of carbon–nitrogen bonds is a new powerful method of organometallic functionalization complementing the "click" reactions of alkynes with azido derivatives that require a catalyst. It opens the route to the introduction of such redox-active organometallics in biomolecules and nanomaterials exemplified by the easy functionalization of aminated silica shown here. Extension of the reactions of electrophilic alkynyl organometallics to various other nanomaterials of interest is underway in our laboratories. The compared reactivity of amines with the cobalticenium, iron, or ruthenium–arene derivatives shows similarities for the unsubstituted derivatives, but the presence of two *ortho* methyl groups on the arene ligand slows down the reaction. These results can be rationalized in light of DFT calculations showing that the reaction mechanism is a two-step process, the rate-limiting second one corresponding to a proton transfer onto the *exo*-cyclic carbon that is sterically protected in the case of the arene *ortho*-substituted complex. The conjugation between the organometallic and enamine groups involves push–pull properties of these colored organometallic *trans*-enamines with fulvalene-iminium and cyclohexadienylidene-iminium mesomeric forms, as reflected by the electrochemical, spectroscopic, and nonlinear optical properties and DFT and TDDFT calculations.

Experimental section

General information

Reagent-grade THF, diethyl ether, and pentane were dried over Na foil and distilled from sodium benzophenone anion under nitrogen immediately prior to use. $PhCH_3$ and dichloromethane were distilled from calcium hydride and distilled under nitrogen prior to use. CH_3CN was dried over P_2O_5 and distilled under nitrogen prior to use. All other solvents and chemicals were used as received. Complex **7** was synthesized as indicated in ref. [13]. ^1H NMR spectra were recorded at 25 °C with a Bruker AC (200, 300, or 600 MHz) spectrometer. ^{13}C NMR spectra were obtained in the pulsed FT mode at 75 or 150 MHz with a Bruker AC 300 or 600 spectrometer. All the chemical shifts are reported in parts per million (δ, ppm) with reference to Me_4Si for the ^1H and ^{13}C NMR spectra. ^{31}P stands for ^{31}P (^1H) in the data, with chemical shifts referenced to H_3PO_4. The ESI mass spectra were recorded using an Applied Biosystems Voyager-DE STR-MALDI-TOF spectrometer. The IR spectra were recorded on an ATI Mattson Genesis series FTIR spectrophotometer. The elemental analyses were performed by the Center of Microanalyses of the CNRS at Lyon Villeurbanne, France. UV/Vis absorption spectra were measured with Perkin–Elmer Lambda 19 UV/Vis spectrometer. Electrochemical measurements (CV) were recorded on a PAR 273 potentiostat under a nitrogen atmosphere. NLO measurements were carried out with a nonresonant incident wavelength of 1.907 μm, obtained by Raman-shifting in a high pressure H_2 of the fundamental 1.064 μm wavelength produced by a Q-switched, mode-locked Nd^{3+}: YAG laser. In the case of EFISH, a short poling electric field (duration 1 μs) pulse in a solvent containing a low dielectric constant ($CHCl_3$) was used to avoid conduction effects in solutions, thus allowing a reliable measurement of the $\mu\beta_{EFISH}$ values of nondissociated ion pairs.[23] The $\mu\beta_{EFISH}$ values reported here are the mean values of four successive measurements performed on the same solution. The value and the sign of $\mu\beta_{EFISH}$ are determined by comparison with the reference solvent ($CHCl_3$).

Synthesis and characterization of the complexes

*Complex **5***: Lithium acetylide ethylenediamine complex (460 mg, 5 mmol, 5 equiv) was added to a suspension of **2** (386 mg, 1 mmol, 1 equiv) in dry THF (10 mL) at 0 °C. The grey mixture was stirred for 1 h at this temperature under N_2 and the color changed from gray to orange. The solvent was removed under vacuum and dry pentane (200 mL) was added in portions to the left solid for extraction. The orange pentane phase and the grey solid were separated by filtration under N_2 and this operation was repeated three times. The combined organic phase was evaporated to give **5** as an orange solid (185.5 mg, yield = 70 %). ^1H NMR (200 MHz, $CDCl_3$), $\delta_{ppm}=1.56$ (s, 6 H; CH_3), 1.86 (s, 1 H), 2.51 (s, 3 H; CH_3), 3.00 (s, 1 H), 4.05 (s, 2 H), 4.05 (s, 5 H; free Cp), 7.26 ppm (s, $CDCl_3$); ^{13}C NMR (50 MHz, $CDCl_3$): $\delta=21.1$ (CH_3), 24.0 (CH_3), 38.1, 38.7, 66.1, 75.1 (free Cp), 78.3, 85.4 ($C\equiv C$), 91.0 ($C\equiv C$), 77.2 ppm ($CDCl_3$); IR (KBr): $\tilde{\nu}=2091$ cm^{-1} ($\nu_{C\equiv C}$); UV/Vis: $\lambda_{max1}=325$, $\lambda_{max2}=405$ nm; ESI-MS: *m/z*: calcd for $C_{16}H_{18}Fe$: 266.1; found: 265.1; elemental analysis calcd (%) for $C_{16}H_{18}Fe$: C 72.20, H: 6.82; found: C 72.40, H 6.90.

*Complex **6***: Lithium acetylideethylene diamine complex (194 mg, 2.11 mmol, 5 equiv) was added to a suspension of **3**[15] (164 mg, 0.422 mmol, 1 equiv) in dry THF (10 mL) at 0 °C, and the mixture was stirred for 1 h at this temperature under N_2. The color changed to pink and the solvent was removed under vacuum. Dry pentane (200 mL) was added portionwise to the left solid for extraction and the pink pentane phase and the grey solid were separated by filtration under N_2. The operation was repeated three times. The combined organic phase was evaporated to give the compound **6** as an pink solid (73.8 mg, yield = 65 %). ^1H NMR (200 MHz, C_6D_6): $\delta=1.85$ (s, 1 H), 2.84 (t, 2 H), 3.22 (t, 1 H), 4.26 (t, 2 H), 4.45 (s, 5 H, free Cp), 5.54 (t, 1 H), 7.16 ppm (s, C_6D_6); ^{13}C NMR (50 MHz, C_6D_6): $\delta=27.04$, 30.38, 66.31 ($C\equiv C$), 75.61 (free Cp), 76.49, 80.75 ($C\equiv C$), 89.92, 128.06 ppm (C_6D_6); IR (KBr): $\tilde{\nu}=2086$ ($\nu_{C\equiv C}$), 809 cm^{-1} (ν_{Cp}); UV/Vis: $\lambda_{max1}=232$, $\lambda_{max2}=310$ nm; ESI-MS: *m/z*: calcd for $C_{13}H_{12}Ru$: 269.3; found: 269.0; elemental analysis calcd for $C_{13}H_{12}Ru$: C 57.98, H 4.49; found: C 57.90, H 4.70.

*Complex **8***: The orange compound **5** (265 mg, 1 mmol, 1 equiv) was dissolved in dry CH_2Cl_2 (10 mL) under N_2 at RT, the green solution of $[CPh_3][PF_6]$ (388 mg, 1 mmol, 1 equiv) in dry CH_2Cl_2 (10 mL) was slowly added to the first solution by syringe under N_2 at RT. The mixture was stirred at this temperature for 1 h, and the color changed to dark red. Then the solvent was removed under vacuum, and the compound was further purified by repeated reprecipitation (6 times, diethyl ether: acetone = 20:1). Complex **8** was collected as an orange solid (279 mg, yield = 68 %). ^1H NMR (300 MHz, CD_3COCD_3): $\delta=2.52$ (s, 3 H; CH_3), 2.70 (s, 6 H; CH_3), 4.44 (s, 1 H; $C\equiv C\text{–}H$), 5.08 (s, 5 H; free Cp), 6.49 (s, 2 H; Ph), 2.06 ppm (m; CD_3COCD_3); ^{13}C NMR (75 MHz, CD_3COCD_3): $\delta=19.34$ (CH_3), 19.51 (CH_3), 76.76 ($C\equiv C$), 79.24 (free Cp), 84.14 ($C\equiv C$), 88.06, 102.17, 103.58, 125.15 (Ph), 29.84, 206.26 ppm (CD_3COCD_3); ^{31}P NMR (121 MHz, CD_3COCD_3): $\delta=-144.14$ ppm (m, PF_6^-); IR (KBr): $\tilde{\nu}=2118$ ($\nu_{C\equiv C}$), 839 cm^{-1} (ν_{PF6}); UV/Vis: $\lambda_{max1}=394$, $\lambda_{max2}=469$ nm; Cyclic voltammograms of $[Fe(Cp)(\eta^6\text{-ethynylmesitylene})][PF_6]$, $Fe^{II/I}$ wave: $E_{1/2(rev)}=-1.26$ V (ΔEp = 30 mV) under the conditions (2 mM) with $[Fe(Cp^*)_2]$ as the internal reference; solvent: DMF; $T=293$ K; supporting electrolyte: $[nBu_4N][PF_6]$ 0.1 M; working and counter electrodes: Pt; reference electrode: Ag; scan rate: 0.200 V.s^{-1}; ESI-MS: *m/z*: calcd for $C_{16}H_{17}Fe^+PF_6$: 265.15; found: 265.08; elemental analysis calcd (%) for $C_{16}H_{17}FePF_6$: C 46.86, H 4.18; found: C 46.97, H 4.26.

*Complex **9***: The pink compound **6** (26.9 mg, 0.1 mmol, 1 equiv) was dissolved in dry CH_2Cl_2 (5 mL) under N_2 at RT, and the green solution of $[CPh_3][PF_6]$ (38.8 mg, 0.1 mmol, 1 equiv) in dry CH_2Cl_2 (5 mL) was slowly added to the first solution by syringe under N_2 at RT. The mixture was stirred at this temperature for 1 h, and the color changed to brown. Then the solvent was removed under vacuum, and the compound was further purified by repeated reprecipitations (6 times diethyl ether/acetone = 20:1) and **9** was collected as a light-yellow solid (29.7 mg, yield = 72 %). ^1H NMR (300 MHz, CD_3COCD_3), $\delta=3.97$ (s, 1 H; $C\equiv C\text{-}H$), 5.63 (s, 5 H; free Cp), 6.43 (t, 1 H; Ph), 6.50 (t, 2 H; Ph), 6.62 (d, 2 H; Ph), 2.06 ppm (m, CD_3COCD_3); ^{13}C NMR (75 MHz, CD_3COCD_3): $\delta=77.95$ ($C\equiv C$), 81.37 (Ph), 82.10 (free Cp), 84.32 ($C\equiv C$), 85.92, 86.09, 88.75 (Ph), 29.84, 206.26 ppm (CD_3COCD_3); IR (KBr): $\tilde{\nu}=2110$ ($\nu_{C\equiv C}$), 836 cm^{-1} (ν_{PF6}); UV/Vis: $\lambda_{max1}=288$, $\lambda_{max2}=342$ nm; ESI-MS: *m/z*: calcd for $C_{13}H_{11}Ru$: 268.30 $[M]^+$; found: 268.99; elemental analysis calcd (%) for $C_{13}H_{11}RuPF_6$: C 37.78, H 2.68; found: C 37.89, H 2.56.

*Complex **11a***: Complex **8** (41.0 mg, 0.1 mmol, 1 equiv) was dissolved in a mixed solvent (10 mL, THF/DIPA = 1:1) and the mixture was stirred under reflux for 24 h. The color changed from light to deep orange. Then the solvent was removed under vacuum to give the enamine **11a** (50.1 mg, yield: 98 %). ^1H NMR (300 MHz, CD_3COCD_3): $\delta=1.27$, 1.29 (d, 12 H; CH_3), 2.44 (s, 3 H; CH_3), 2.63 (s, 6 H; CH_3), 3.93 (m, 2 H; CH/*i*Pr), 4.84 (s, 5 H; free Cp), 5.22, 5.27 (d, $J=15.0$, 1 H; C=C), 6.22 (s, 2 H; Ph), 6.85, 6.90 (d, $J=15.0$, 1 H; C=C), 2.06 ppm (m, CD_3COCD_3); ^{13}C NMR (75 MHz, CD_3COCD_3): $\delta = 18.63$ (CH_3), 18.94 (CH_3), 20.97 (CH_3/*i*Pr), 46.55 (CH/*i*Pr), 77.50 (free Cp), 85.08 (CH=CH), 88.55, 95.89, 99.00, 125.16 (Ph), 141.40 (CH=CH), 29.84, 206.26 ppm (CD_3COCD_3); ^{31}P NMR (121 MHz, CD_3COCD_3), $\delta = -144.14$ ppm (m, PF_6^-); IR (KBr): $\tilde{\nu} = 1586$ ($\nu_{CH=CH}$), 841 cm^{-1} (ν_{PF6}); UV/Vis: $\lambda_{max1} = 382$, $\lambda_{max2} = 435$ nm; Cyclic voltammograms of **11a**, $Fe^{II/I}$ wave: $E_{1/2(rev)} = -1.51$ V ($\Delta Ep = 70$ mV) under the conditions (2 mM) with $[Fe(Cp^*)_2]$ as the internal reference; solvent: DMF; *T*: 293 K; supporting electrolyte: $[nBu_4N][PF_6]$ 0.1 M; working and counter electrodes: Pt; reference electrode: Ag; scan rate: 0.200 Vs^{-1}. ESI-MS: *m/z*: calcd for $C_{22}H_{32}FeN^+$: 366.3 $[M]^+$; found: 366.1; elemental analysis calcd (%) for $C_{22}H_{32}FeNPF_6$: C 51.68, H 6.31, N 2.74; found: C 51.70, H 6.17, N 2.57.

Complex ***11b***: Complex **8** (41.0 mg, 0.1 mmol, 1 equiv) was dissolved in a mixed solvent 10 mL ($THF/Et_2NH = 1:1$) and the mixture was stirred under 35 °C for 24 h. The color changed from light to deep orange. Then the solvent was removed under vacuum to give the enamine **11b** (46.9 mg, yield = 97%). ^1H NMR (300 MHz, CD_3COCD_3), $\delta = 1.23$ (t, 6H; CH_3), 2.44 (s, 3H; CH_3), 2.62 (s, 6H; CH_3), 3.61 (m, 4H; CH_2), 4.85 (s, 5H; free Cp), 5.13, 5.18 (d, *J* = 15.0, 1H; HC=CH), 6.21 (s, 2H; Ph), 6.85, 6.90 (d, *J* = 15.0, 1H; HC=CH), 2.05 ppm (m, CD_3COCD_3); ^{13}C NMR (75 MHz, CD_3COCD_3): $\delta = 12.70$ (CH_3/Et), 19.18 (CH_3), 21.10 (CH_3), 45.34 (CH_2/Et), 77.73 (free Cp), 85.36 (CH=CH), 88.78, 96.14, 96.55, 102.75 (Ph), 145.61 (CH=CH), 29.84, 206.26 ppm (CD_3COCD_3); ^{31}P NMR (121 MHz, CD_3COCD_3): $\delta = -144.14$ ppm (m, PF_6^-); IR (KBr): $\tilde{\nu} = 1610$ ($\nu_{CH=CH}$), 840 cm^{-1} (ν_{PF6}); UV/Vis: $\lambda_{max1} = 323$, $\lambda_{max2} = 416$, $\lambda_{max3} = 514$ nm; ESI-MS: *m/z*: calcd for $C_{20}H_{28}FeN^+$: 338.29 $[M]^+$; found: elemental analysis calcd (%) for $C_{20}H_{28}FeNPF_6$: C 49.71, H 5.84, N 2.90; found: C 49.40, H 6.11, N 2.67.

Complex ***12a***: Complex **9** (16.5 mg, 0.04 mmol, 1 equiv) was dissolved in a mixed solvent 10 mL (THF/DIPA = 1:1) and the mixture was stirred at 35 °C for 24 h, and the color changed from light yellow to orange. Then the solvent was removed under vacuum to give the enamine compound **12a** (19.5 mg, yield = 95%). ^1H NMR (300 MHz, CD_3COCD_3): $\delta = 1.34$, 1.36 (d, 12H; CH_3), 3.81 (m, 2H; CH/*i*Pr), 5.95, 5.00 (d, *J* = 15.0, 1H; HC=CH), 5.31 (s, 5H; freeCp), 6.00 (t, 1H; Ph), 6.14 (t, 2H; Ph), 6.40 (d, 2H; Ph), 7.37, 7.41 (d, *J* = 18.0, 1H; HC=CH), 2.06 ppm (m, CD_3COCD_3); ^{13}C NMR (75 MHz, CD_3COCD_3): $\delta = 18.88$ (CH_3/*i*Pr), 46.57 (CH/*i*Pr), 76.63 (Ph), 80.32 (free Cp), 80.44, 80.66, 86.14 (Ph), 86.89 (C=C), 138.00 (C=C), 29.84, 206.26 ppm (CD_3COCD_3); IR (KBr): $\tilde{\nu} = 1618$ ($\nu_{C=C}$), 837 cm^{-1} (ν_{PF6}); UV/Vis: $\lambda_{max1} = 229$, $\lambda_{max2} = 339$, $\lambda_{max3} = 367$ nm. ESI-MS: *m/z*: calcd for $C_{19}H_{26}RuN^+$: 369.49 $[M]^+$; found: 370.11; elemental analysis calcd (%) for $C_{19}H_{26}RuN^+PF_6$: C 44.36, H 5.09, N 2.72; found: C 44.67, H 5.23, N 2.87.

Complex ***12b***: Complex **9** (16.5 mg, 0.04 mmol, 1 equiv) was dissolved in a mixed solvent (10 mL, $THF/Et_2NH = 1:1$) and the mixture was stirred at 35 °C for 1 h. The color changed from light yellow to orange. Then the solvent was removed under vacuum to give the enamine compound **12b** (18.7 mg, yield = 96%). ^1H NMR (300 MHz, CD_3COCD_3): $\delta = 1.17$ (t, 6H; CH_3), 3.29 (m, 4H; CH_2), 4.81, 4.86 (d, *J* = 15.0, 1H; HC=CH), 5.32 (s, 5H; free Cp), 6.00 (t, 1H; Ph), 6.15 (t, 2H; Ph), 6.36 (d, 2H; Ph), 7.33, 7.37 (d, *J* = 12.0, 1H; HC=CH), 2.05 ppm (m, CD_3COCD_3); ^{13}C NMR (75 MHz, CD_3COCD_3): $\delta = 12.67$ (CH_3), 46.00 (CH_2), 78.29 (free Cp), 79.68 (free Cp), 82.13, 82.15, 84.58 (Ph), 86.82 (C=C), 143.50 (C=C), 29.84, 206.26 ppm (CD_3COCD_3); IR (KBr): $\tilde{\nu} = 1626$ ($\nu_{C=C}$), 837 cm^{-1} (ν_{PF6}); UV/Vis: $\lambda_{max1} = 343$, $\lambda_{max2} = 363$ nm; ESI-MS: *m/z*: calcd for $C_{17}H_{22}RuN$: 341.43 $[M]^+$; found: 342.08; elemental analysis calcd (%) for $C_{17}H_{22}RuN^+PF_6$: C 41.98, H 4.56, N 2.88; found: C 41.67, H 4.33, N 2.87.

Derivatization of aminosilica nanoparticles 13 by reaction with 7

MT-ST silica nanoparticles (SiO_2NPs, 12 nm diameter) were purchased from Nissan Chemical. SiO_2NPs (3.78 g) were precipitated from MeOH (the purchased solution) by adding toluene (10 mL) and washed four times by centrifugation followed by redispersion in toluene. 3-(Trimethoxysilyl)propylamine (0.24 mL) in toluene (10 mL) was added to the SiO_2NPs suspension in toluene followed by heating at 78 °C for 24 h. The SiO_2NPs were then washed four times by centrifugation and redispersion in toluene and then four times with methanol. The solvent layer was colorless after centrifuging the SiO_2NPs out of solution. The left white solid **13** was dispersed in CH_2Cl_2/acetone (1:1) by sonication for further experimental use. Then **13** (500 mg) in CH_2Cl_2/acetone (10 mL, 1:1) was reacted with **7** (0.2 g) under sonication for 18 h at 50 °C. The color of the mixture changed from yellow to deep violet during the sonication. The resulting suspension was centrifuged and the solution was decanted, the remaining deep violet precipitate was washed with CH_2Cl_2 (three times) with successive centrifugation, decantation and re-dispersion under sonication. The precipitate was dried under vacuum, and deep violet Co-SiO_2NPs, **14**, (320 mg) were obtained. IR (KBr) of **13**: $\tilde{\nu} = 1106$ (ν_{Si-O}), 3368, 3305 cm^{-1} (ν_{NH2}); IR (KBr) of **14**: $\tilde{\nu} = 1105$ (ν_{Si-O}), 3275 (ν_{NH}), 1621 cm^{-1} ($\nu_{CH=CH}$), 832 cm^{-1} (ν_{PF6}); UV/Vis of **14**: $\lambda_{max1} = 610$, $\lambda_{max2} = 502$, $\lambda_{max3} = 391$, $\lambda_{max4} = 310$ nm; cyclic voltammetry of **14** obtained at a Pt electrode at 25 °C in DMF; supporting electrolyte: $[nBu_4N][PF_6]$. $Co^{III/II}$ wave: $E_{1/2}(rev) = -0.94$ V ($\Delta E_p = 65$ mV) vs. $[Fe(Cp^*)_2]^{0/+}$.

Computational details

DFT calculations were carried out using the Gaussian 09 package,[25] employing the B3PW91 functional,[26] and using a standard double-ξ basis set, namely the LANL2DZ, augmented with polarization functions on all atoms.[27] Analytical frequency calculations have been performed on all the computed extrema to characterize their nature and to calculate their free energy at 298 K. The Wiberg bond indices and natural charge analysis have been computed with the NBO 5.0 program.[28] The composition of the molecular orbitals was calculated using the AOMix program.[29] The UV/Vis transitions were calculated by means of time-dependent DFT (TDDFT) calculations at the same level of theory. Only transitions with non-negligible oscillator strengths are reported and discussed. Representation of the molecular structures was done using the Gaussview program.[30] The UV/Vis spectra were simulated from the computed TDDFT transitions and their oscillator strengths by using the SWizard program,[31] each transition being associated with a Gaussian function of half-height width equal to 3000 cm^{-1}. More sophisticated calculations using the ωB97XD functional,[32] which includes dispersion effects, associated with the triple-ξ polarized basis set, namely the Def2TZVP,[33] led to the same results concerning the reaction pathways and activation energies. When inclusion of solvent corrections is specified, it corresponds to the use of the PCM model.[34]

Acknowledgements

The authors declare no competing financial interests. Financial support from the China Scholarship Council (CSC), People's Republic of China (Ph.D. grant to Y.W.), the Universities of Bordeaux and Rennes 1, the Ecole Nationale Supérieure (ENS) de Cachan, the Institut Universitaire de France (IUF: J.Y.S. and D.A.), and the Centre National de la Recherche Scientifique (CNRS) is gratefully acknowledged.

Keywords: alkynes · Co · enamines · green chemistry · push–pull

[1] a) P. Nguyen, P. Gomez-Elipe, C. Manners, *Chem. Rev.* **1999**, *99*, 1515–1528; b) I. Manners, *Science* **2001**, *294*, 1664–1666; c) G. R. Whittel, I. Manners, *Adv. Mater.* **2007**, *19*, 3239–3468; d) G. R. Whittel, M. D. Hager, U. S. Schubert, I. Manners, *Nat. Mater.* **2011**, *10*, 176–188; e) J. C. Eloi, D. A. Rider, G. Cambridge, G. R. Whittel, M. A. Winnik, I. Manner, *J. Am. Chem. Soc.* **2011**, *133*, 8903–8913; f) F. H. Schacher, P. A. Rupar, I. Manners, *Angew. Chem.* **2012**, *124*, 8020–8044; *Angew. Chem. Int. Ed.* **2012**, *51*, 7898–7921.

[2] H. C. Kolb, M. G. Finn, K. B. Sharpless, *Angew. Chem.* **2001**, *113*, 2056–2075; *Angew. Chem. Int. Ed.* **2001**, *40*, 2004–2021.

[3] a) J.-F. Lutz, *Angew. Chem.* **2007**, *119*, 1036–1043; *Angew. Chem. Int. Ed.* **2007**, *46*, 1018–1025; b) W. H. Binder, R. Sachenhofer, *Macromol. Rapid Commun.* **2007**, *28*, 15–54; c) J. E. Moses, A. D. Moorehouse, *Chem. Soc. Rev.* **2007**, *36*, 1249–1262; d) C. R. Becer, R. Hoogenboom, U. S. Schubert, *Angew. Chem.* **2009**, *121*, 4998–5006; *Angew. Chem. Int. Ed.* **2009**, *48*, 4900–4908.

[4] a) D. Fournier, R. Hoogenboom, U. S. Schubert, *Chem. Soc. Rev.* **2007**, *36*, 1369–1380; b) M. Meldal, C. W. Torne, *Chem. Rev.* **2008**, *108*, 2952–3015; c) J. E. Hein, V. V. Fokin, *Chem. Soc. Rev.* **2010**, *39*, 1302–1315; d) L. Liang, D. Astruc, *Coord. Chem. Rev.* **2011**, *255*, 2933–2945.

[5] S. A. Lawrence, *Amines: Syntheses, Properties and Applications*, Cambridge University Press, Cambridge, **2004**.

[6] a) F. Alonso, I. P. Beletskaya, M. Yus, *Chem. Rev.* **2004**, *104*, 3079–3160; b) R. Séverinand, S. Doye, *Chem. Soc. Rev.* **2007**, *36*, 1407–1420; c) T. E. Müller, K. C. Hulzsch, M. Yus, F. Foubelo, M. Tada, *Chem. Rev.* **2008**, *108*, 3795–3892.

[7] General reviews of nucleophilic addition to electron-deficient carbon–carbon multiple bonds: a) *Comprehensive Organic Synthesis, Vol. 4* (Eds.: B. M. Trost, I. Fleming), Pergamon, Oxford, **1991**; b) F. A. Carey, R. J. Sundberg, *Advanced Organic Chemistry, 5th ed.*, Part B, Springer, New York, **2007**, pp. 183–200; c) M. B. Smith, J. March, *March's Advanced Organic Chemistry, 6th ed.*, Wiley, New York, **2007**, pp. 1130–1132.

[8] Recent examples of reactions of nucleophiles with haloalkynes: a) T. B. Poulsen, L. Barnardi, J. Aleman, J. Overgaard, K. A. Jorgensen, *J. Am. Chem. Soc.* **2007**, *129*, 441–449; b) A. Trofimov, N. Cherniak, V. Gevorgyan, *J. Am. Chem. Soc.* **2008**, *130*, 13538–13539; c) B. A. Trofimov, A. G. Malkina, O. A. Shemyakina, V. V. Nosyreva, A. P. Borisova, S. S. Khutsishvili, L. B. Krivdin, *Synthesis* **2009**, 3136–3142; d) M. Yamagishi, K. Nishigai, T. Hata, H. Urabe, *Org. Lett.* **2011**, *13*, 4873–4875.

[9] Intramolecular amination of haloalkynes: a) Z. Miao, M. Xu, B. Hoffmann, B. Bernet, A. Vasella, *Helv. Chim. Acta* **2005**, *88*, 1885–1912; b) V. N. Elokhina, A. S. Nakhmanovich, *Russ. J. Org. Chem.* **2009**, *45*, 226–228.

[10] Hydroamination of benzoylethynyltetrahydroindoles: a) L. N. Sobenina, D. N. Tomilin, O. V. Petrova, I. A. Ushakov, A. Mikhaleva, B. A. Trofimov, *Synthesis* **2010**, *14*, 2468–2474; b) L. N. Sobenina, D. N. Tomilin, D. A. Ushakov, A. Mikhaleva, B. A. Trofimov, *Synthesis* **2012**, *44*, 2084–2090.

[11] Nucleophilic attacks on ligands often proceed according to charge control,[12a] but orbital control has a priority when it is in conflict with charge control. a) S. G. Davies, M. L. H. Green, D. M. P. Mingos, *Tetrahedron* **1978**, *34*, 20–50; b) D. Astruc, P. Michaud, A. Madonik, J.-Y. Saillard, R. Hoffmann, *Nouv. J. Chim.* **1985**, *9*, 41–50.

[12] Reactions of substituted cyclohexadienyl complexes with a trityl salt or *N*-bromosuccidimide had been reported to give a mixture of *endo*-hydride abstraction providing the desired substituted complex and *exo*-substituent abstraction giving back the starting material: a) I. U. Khand, P. L. Pauson, W. E. Watts, *J. Chem. Soc. C* **1969**, 2024–2030; b) A. N. Nesmeyanov, N. A. Vol'kenau, L. S. Shilovtseva, V. A. Petrakovich, *J. Organomet. Chem.* **1975**, *85*, 365–373; In one case, it had been found that the *exo*-substituent abstraction by Ph_3C^+ occurring at room temperature could be suppressed by conducting the reaction at low temperature, which selectively yielded the *endo*-hydride abstraction compound: c) A. Madonik, D. Astruc, *J. Am. Chem. Soc.* **1984**, *106*, 2437–2439; d) D. Mandon, L. Toupet, D. Astruc, *J. Am. Chem. Soc.* **1986**, *108*, 1320–1321.

[13] a) M. Wildschek, C. Rieker, P. Jaitner, H. Schottenberger, K. E. Schwarzhans, *J. Organomet. Chem.* **1990**, *396*, 355–361; b) Upon repeating this synthesis, we find by ^1H NMR spectroscopic analysis that the tentative hydride abstraction by $[Ph_3C][PF_6]$ provides the expected product **7** but also 10% of *exo*-ethynyl cleavage giving back the starting unsubstituted cobalticenium salt **1** that can be easily separated by column chromatography.

[14] a) A. N. Nesmeyanov, N. A. Vol'kenau, I. N. Bolesova, *Tetrahedron Lett.* **1963**, *4*, 1725–1729; b) A. N. Nesmeyanov, N. A. Vol'kenau, I. N. Bolesova, *Dokl. Akad. Nauk SSSR* **1966**, *166*, 607; c) C. Moinet, E. Román, D. Astruc, *J. Electroanal. Chem. Interfacial Electrochem.* **1981**, *121*, 241–246; d) J. Ruiz, M. Lacoste, D. Astruc, *J. Am. Chem. Soc.* **1990**, *112*, 5471–5483.

[15] a) R. A. Zelonka, M. C. Baird, *J. Organomet. Chem.* **1972**, *44*, 383–389; b) R. A. Zelonka, M. C. Baird, *J. Can. Chim.* **1972**, *50*, 3063–3072; c) T. P. Gill, K. R. Mann, *Organometallics* **1982**, *1*, 485–488; d) N. Oshima, H. Suzuki, Y. Morooka, *Inorg. Chem.* **1986**, *25*, 3407–3412; e) M. O. Albers, D. C. Liles, D. J. Robinson, A. Shaver, E. Singleton, *J. Chem. Soc. Chem. Commun.* **1986**, 645–647; f) M. O. Albers, D. J. Robinson, A. Shaver, E. Singleton, *Organometallics* **1986**, *5*, 2199–2205; g) M. O. Albers, D. C. Liles, D. J. Robinson, A. Shaver, E. Singleton, *Organometallics* **1987**, *6*, 2347–2354; h) E. P. Kündig, P. Jeger, G. Bernardinelli, *Inorg. Chim. Acta* **2004**, *357*, 1909–1919.

[16] a) A. Rapakousiou, C. Mouche, M. Duttine, J. Ruiz, D. Astruc, *Eur. J. Inorg. Chem.* **2012**, 5071–5077; b) A. Rapakousiou, Y. Wang, C. Belin, N. Pinaud, J. Ruiz, D. Astruc, *Inorg. Chem.* **2013**, *52*, 6685–6693; c) A. Rapakousiou, Y. Wang, J. Ruiz, D. Astruc, *J. Inorg. Organomet. Polym. Mater.* **2014**, *24*, 107–113; d) Y. Wang, A. Rapakousiou, C. Latouche, J.-C. Daran, A. Singh, I. Ledoux-Rak, J. Ruiz, J.-Y. Saillard, D. Astruc, *Chem. Commun.* **2013**, *49*, 5862–5864.

[17] K. Lammertsma, B. V. Prasad, *J. Am. Chem. Soc.* **1994**, *116*, 642–650.

[18] a) J.-R. Hamon, D. Astruc, P. Michaud, *J. Am. Chem. Soc.* **1981**, *103*, 758–766; b) B. Gloaguen, D. Astruc, *J. Am. Chem. Soc.* **1990**, *112*, 4607–4609; c) The pK_a of the isostructural complexes $[M(\eta^6\text{-arene})(Cp)][PF_6]$, Fe vs. Ru, are the same, which indicates that the charge delocalization of the *exo*-cyclic carbon is the same in the isostructural Fe and Ru complexes. H. A. Trujillo, C.-M. Casado, J. Ruiz, D. Astruc, *J. Am. Chem. Soc.* **1999**, *121*, 5674–5686.

[19] R. Hoffmann, P. Hofman, *J. Am. Chem. Soc.* **1976**, *98*, 598–604.

[20] L. Ren, J. Zhang, C. G. Hardy, D. Doxie, B. Fleming, C. Tang, *Macromolecules* **2012**, *45*, 2267–2275.

[21] a) B. F. Levine, C. G. Bethea, *J. Chem. Phys.* **1975**, *63*, 2666–2669; b) I. Ledoux, J, Zyss, *Chem. Phys.* **1982**, *73*, 203–213.

[22] a) P. D. Maker, *Phys. Rev. A* **1970**, *1*, 923–951; b) K. Clays, A. Persoons, *Phys. Rev. Lett.* **1991**, *66*, 2980–2983.

[23] V. Alain, M. Blanchard-Desce, I. Ledoux-Rak, J. Zyss, *Chem. Commun.* **2000**, 353–354.

[24] a) A. Vidal, E. Papirer, *Hydroxyl Groups on Silica Surfaces: Chemical Reactivity* (Ed.: A. P. Legrand), Wiley, Chichester, **1998**, pp. 285–312; b) T. Kusamoto, J. Ruiz, D. Astruc, *New J. Chem.* **2009**, *33*, 2204–2207; c) C. A. Beasley, R. W. Murray, *Langmuir* **2009**, *25*, 10370–10375.

[25] Gaussian 09 (Revision A.02), M. J. Frisch, G. W. Trucks, H. B. Schlegel, G. E. Scuseria, M. A. Robb, J. R. Cheeseman, G. Scalmani, V. Barone, B. Mennucci, G. A. Petersson, H. Nakatsuji, M. Caricato, X. Li, H. P. Hratchian, A. F. Izmaylov, J. Bloino, G. Zheng, J. L. Sonnenberg, M. Hada, M. Ehara, K. Toyota, R. Fukuda, J. Hasegawa, M. Ishida, T. Nakajima, Y. Honda, O. Kitao, H. Nakai, T. Vreven, J. A., Jr., Montgomery, J. E. Peralta, F. Ogliaro, M. Bearpark, J. J. Heyd, E. Brothers, K. N. Kudin, V. N. Staroverov, R. Kobayashi, J. Normand, K. Raghavachari, A. Rendell, J. C. Burant, S. S. Iyengar, J. Tomasi, M. Cossi, N. Rega, J. M. Millam, M. Klene, J. E. Knox, J. B. Cross, V. Bakken, C. Adamo, J. Jaramillo, R. Gomperts, R. E. Stratmann, O. Yazyev, A. J. Austin, R. Cammi, C. Pomelli, J. W. Ochterski, R. L. Martin,

K. Morokuma, V. G. Zakrzewski, G. A. Voth, P. Salvador, J. J. Dannenberg, S. Dapprich, A. D. Daniels, O. Farkas, J. B. Foresman, J. V. Ortiz, J. Cioslowski, D. J. Fox, Gaussian, Inc., Wallingford, CT, **2009**.

[26] a) *Electronic Structure of Solids '91* (Eds.: P. Ziesche, H. Eschrig), Akademie Verlag, Berlin, **1991**; b) A. D. Becke, *J. Chem. Phys.* **1993**, *98*, 5648–5652.

[27] a) T. H. Dunning, Jr., P. J. Hay, *Methods of Electronic Structure Theory* (Ed.: H. F. Schaeffer), Plenum, New York, **1977**; b) P. J. Hay, W. R. Wadt, *J. Chem. Phys.* **1985**, *82*, 270–283; c) P. J. Hay, W. R. Wadt, *J. Chem. Phys.* **1985**, *82*, 284–298; d) P. J. Hay, W. R. Wadt, *J. Chem. Phys.* **1985**, *82*, 299–310; e) A. Schafer, H. Horn, R. Ahlrichs, *J. Chem. Phys.* **1992**, *97*, 2571–2577.

[28] E. D. Glendening, J. K. Badenhoop, A. E. Reed, J. E. Carpenter, J. A. Bohmann, C. M. Morales, F. Weinhold, NBO 5.0, Theoretical Chemistry Institute, University of Wisconsin: Madison, WI, **2001**, http://www.chem.wisc.edu/nbo5.

[29] S. I. Gorelsky, AOMix: Program for Molecular Orbital Analysis, **2009**, www.sg-chem.net.

[30] R. Dennington, T. Keith, J. Millam, GaussView, Version 5, Semichem Inc., Shawnee Mission KS, **2009**.

[31] S. I. Gorelsky, Swizard program, revision 4.5 www.sg-chem.net/swizard.

[32] J.-D. Chai, M. Head-Gordon, *Phys. Chem. Chem. Phys.* **2008**, *10*, 6615–6620.

[33] F. Weigend, R. Ahlrichs, *Phys. Chem. Chem. Phys.* **2005**, *7*, 3297–3305.

[34] a) V. Barone, M. Cossi, J. Tomasi, *J. Chem. Phys.* **1997**, *107*, 3210–3221; b) M. Cossi, G. Scalmani, N. Rega, V. Barone, *J. Chem. Phys.* **2002**, *117*, 43–54.

Received: January 29, 2014